New Journal of Physics
The open-access journal for physics

The trapped two-dimensional Bose gas: from Bose–Einstein condensation to Berezinskii–Kosterlitz–Thouless physics

Z Hadzibabic[1,2], P Krüger[1,3,4], M Cheneau[1], S P Rath[1] and J Dalibard[1,5]

[1] Laboratoire Kastler Brossel, CNRS, École Normale Supérieure, 24 rue Lhomond, 75005, Paris, France
[2] Cavendish Laboratory, University of Cambridge, Cambridge CB3 0HE, UK
[3] Kirchhoff Institut für Physik, Universität Heidelberg, 69120 Heidelberg, Germany
[4] Midlands Centre for Ultracold Atoms, School of Physics and Astronomy, University of Nottingham, Nottingham NG7 2RD, UK
E-mail: jean.dalibard@lkb.ens.fr

New Journal of Physics **10** (2008) 045006 (22pp)
Received 7 December 2007
Published 30 April 2008
Online at http://www.njp.org/
doi:10.1088/1367-2630/10/4/045006

Abstract. We analyze the results of a recent experiment with bosonic rubidium atoms harmonically confined in a quasi-two-dimensional (2D) geometry. In this experiment a well-defined critical point was identified, which separates the high-temperature normal state characterized by a single component density distribution, and the low-temperature state characterized by a bimodal density distribution and the emergence of high-contrast interference between independent 2D clouds. We first show that this transition cannot be explained in terms of conventional Bose–Einstein condensation of the trapped ideal Bose gas. Using the local density approximation (LDA), we then combine the mean-field (MF) Hartree–Fock theory with the prediction for the Berezinskii–Kosterlitz–Thouless (BKT) transition in an infinite uniform system. If the gas is treated as a strictly 2D system, the MF predictions for the spatial density profiles significantly deviate from those of a recent quantum Monte Carlo (QMC) analysis. However, when the residual thermal excitation of the strongly confined

[5] Author to whom any correspondence should be addressed.

degree of freedom is taken into account, excellent agreement is reached between the MF and the QMC approaches. For the interaction strength corresponding to the experiment, we predict a strong correction to the critical atom number with respect to the ideal gas theory (factor ∼2). Quantitative agreement between theory and experiment is reached concerning the critical atom number if the predicted density profiles are used for temperature calibration.

Contents

1. Introduction

As first noticed by Peierls [1], collective physical phenomena in an environment with a reduced number of dimensions can be dramatically changed with respect to our experience in three dimensions (3D). The example of Bose–Einstein condensation in a uniform gas is a good illustration of the crucial role of dimensionality. In 3D, condensation occurs at a finite temperature, and the phase of the macroscopic wavefunction exhibits long range order [2]. In 2D, such long range order is destroyed by thermal fluctuations at any finite temperature, both for an ideal and for an interacting Bose gas [3, 4].

In the presence of repulsive interactions between particles, a uniform 2D Bose gas can nevertheless undergo a phase transition from a normal to a superfluid state at a finite critical temperature. This transition was predicted by Berezinskii [5] and by Kosterlitz and Thouless [6] (BKT), and it has been observed in several macroscopic quantum systems, such as helium films adsorbed on a substrate [7]. The superfluid state exhibits quasi-long range order, such that the

one-body correlation function decays algebraically at large distance. By contrast the decay is exponential in the normal phase.

The recent advances in the manipulation of quantum atomic gases have made it possible to address the properties of low-dimensional Bose gases with novel tools and diagnostic techniques [8]–[18] (for recent reviews, see [19, 20]). A recent cold atom experiment also addressed the BKT problem by realizing a 2D array of atomic Josephson junctions [21]. All these systems bring new questions, since one is now dealing with a harmonically trapped, instead of a uniform, fluid. In particular, due to a different density of states, even in 2D one expects to recover the Bose–Einstein condensation phenomenon in the ideal Bose gas case [22]. The total number of atoms in the excited states of the trap is bounded from above, and a macroscopic population of the ground state appears for large enough atom numbers. However real atomic gases do interact. It is therefore a challenging question to understand whether in the presence of atomic interactions, a trapped Bose gas will undergo a BKT superfluid transition like in the uniform case, or whether conventional Bose–Einstein condensation will take place, as for an ideal system.

In recent experiments performed in our laboratory [17, 18], a gas of rubidium atoms was trapped using a combination of a magnetic trap providing harmonic confinement in the xy-plane, and an optical lattice, ensuring that the third degree of freedom (z) of the gas was frozen. The analysis of the atomic density profile revealed a critical point, between a high temperature phase with a single component density distribution, and a low temperature phase with a clear bimodal distribution [18]. This critical point also corresponded to the onset of clearly visible interferences between independent gases, which were used to study the coherence properties of the system [17]. Surprisingly, the density profile of the normal component was observed to be close to a Gaussian all the way down (in temperature) to the critical point. This density profile is strikingly different from the one expected for the ideal gas close to the BEC critical temperature. Furthermore, if the width of the observed quasi-Gaussian distribution is interpreted as an empirical measure of the temperature, this leads to a critical atom number at a given temperature which is about five times larger than that needed for conventional Bose–Einstein condensation in the ideal gas. These two facts showed that, in sharp contrast to the 3D case, interactions in 2D cannot be treated as a minor correction to the ideal gas BEC picture, but rather qualitatively change the behavior of the system.

The main goal of the present paper is to analyze this critical point. We start in section 2 with a brief review of the properties of an ideal Bose gas in the uniform case and in the case of harmonic confinement. In section 3, we adapt the ideal gas treatment to the experimental geometry of [18], and provide a detailed calculation showing that the experimental results cannot be explained by this theory. Next, in section 4, we take interactions into account at the mean-field (MF) level and we combine this analysis with the numerically known threshold for the BKT transition in the uniform case [23]. We first present a MF treatment for a strictly 2D gas. For the parameter range explored experimentally, it leads to a critical atom number in good agreement with the prediction of the most recent quantum Monte Carlo (QMC) calculations [24]. However the predicted MF density profiles significantly differ from the QMC ones in the vicinity of the critical point. In a second step, we take into account the residual excitation of the z motion in the MF model and we obtain excellent agreement with the QMC calculation. The predicted density distribution near the critical point has a quasi-Gaussian shape and the 'empirical' temperature extracted from this distribution is in fact somewhat lower than the real temperature. Taking this into account we obtain good quantitative agreement between

experimental results and theoretical predictions. Finally we summarize our findings and discuss the connection between the BEC and the BKT transition in a 2D gas. While in a uniform, infinite system only the latter can occur at finite temperature, in a trapped gas both are possible, and the BEC transition can be viewed as a special, non-interacting limit of the more general BKT behavior.

2. Bose–Einstein condensation in an ideal 2D Bose gas

This section is devoted to a review of well-known results concerning the ideal Bose gas in 2D. We first address the case of a uniform system at the thermodynamic limit, and we then consider a gas confined in a harmonic potential.

2.1. The uniform case

In the thermodynamic limit a uniform, ideal Bose gas does not undergo Bose–Einstein condensation when the temperature T is reduced, or the 2D spatial density n is increased. Bose–Einstein statistics leads to the following relation between the phase space density $D = n\lambda^2$ and the fugacity $Z = \exp(\beta\mu)$

$$D = g_1(Z), \qquad g_\alpha(Z) = \sum_{j=1}^{\infty} Z^j / j^\alpha. \tag{1}$$

Here $\lambda = \hbar(2\pi/(mk_\mathrm{B}T))^{1/2}$ is the thermal wavelength, m is the atomic mass, $\beta = 1/(k_\mathrm{B}T)$ and μ is the chemical potential. The function $g_\alpha(Z)$ is the polylogarithm, that takes the simple form $g_1(Z) = -\ln(1-Z)$ for $\alpha = 1$. Because $g_1(Z) \to +\infty$ when $Z \to 1$, (1) has a solution in Z for any value of D. Hence no singularity appears in the distribution of the population of the single particle levels, even when the gas is strongly degenerate ($D \gg 1$). This is to be contrasted with the well-known 3D case: the relation $D^{(3\mathrm{D})} = g_{3/2}(Z)$ ceases to have a solution for a phase space density above the critical value $D_\mathrm{c}^{(3\mathrm{D})} = g_{3/2}(1) \simeq 2.612$, where the 3D Bose–Einstein condensation phenomenon takes place.

2.2. The ideal 2D Bose gas in harmonic confinement

We now consider an ideal gas confined in a harmonic potential $V(\mathbf{r}) = m\omega^2 r^2/2$. We assume that thermal equilibrium has been reached, so that the population of each energy level is given by Bose–Einstein statistics. Since the chemical potential μ is always lower than the energy $\hbar\omega$ of the ground state of the trap, the number of atoms N' occupying the excited states of the trap cannot exceed the critical value $N_\mathrm{c}^{(\mathrm{id})}$

$$N_\mathrm{c}^{(\mathrm{id})} = \sum_{j=1}^{+\infty} \frac{j+1}{\exp(j\beta\hbar\omega) - 1}\,. \tag{2}$$

This expression can be evaluated in the so-called *semi-classical limit* $k_\mathrm{B}T \gg \hbar\omega$ by replacing the discrete sum by an integral over the energy ranging from 0 to $+\infty$ [22]:

$$N_\mathrm{c}^{(\mathrm{id})} = \left(\frac{k_\mathrm{B}T}{\hbar\omega}\right)^2 g_2(1), \tag{3}$$

with $g_2(1) = \pi^2/6$. This result also holds in the case of an anisotropic harmonic potential in the xy-plane, in which case ω is replaced by the geometric mean $\bar{\omega} = \sqrt{\omega_x \omega_y}$, where ω_x, ω_y are the two eigenfrequencies of the trap. The saturation of the number of atoms in the excited states is a direct manifestation of Bose–Einstein condensation: any total atom number N above $N_c^{(\mathrm{id})}$ must lead to the accumulation of at least $N - N_c^{(\mathrm{id})}$ in the ground state of the trap.

Equation (3) is very reminiscent of the result for the harmonically trapped 3D gas, where the saturation number is $N_c^{(3\mathrm{D,id})} = (k_B T/(\hbar\omega))^3\, g_3(1)$. However, an important difference arises between the 2D and the 3D cases for the spatial density profile. In 3D the phase space density in $\mathbf{r}$ is given by $D^{(3\mathrm{D})}(\mathbf{r}) = g_{3/2}(Z\mathrm{e}^{-\beta V(\mathbf{r})})$ in the limit $k_B T \gg \hbar\omega$. The threshold for Bose–Einstein condensation is reached for $Z = 1$; at this point N is equal to the critical number $N_c^{(3\mathrm{D,id})}$ and simultaneously the phase space density at the center of the trap $D^{(3\mathrm{D})}(0)$ equals the critical value $g_{3/2}(1)$. This allows for a simple connection between the BEC thresholds for a homogeneous gas and for a trapped system in the semi-classical limit $k_B T \gg \hbar\omega$. In 2D, such a simple connection between global properties (critical atom number $N_c^{(\mathrm{id})}$) and local properties (critical density at center $n(0)$) does not exist. Indeed the semi-classical expression of the 2D phase space density is

$$D(\mathbf{r}) = g_1(Z\mathrm{e}^{-\beta V(\mathbf{r})}). \tag{4}$$

Because $g_1(1) = +\infty$ this leads to a diverging value at the center of the trap when Z approaches 1. Therefore, although the integral of $D(\mathbf{r})$ over the whole space converges for $Z = 1$ and allows to recover (3), the semiclassical result (4) cannot be used to derive a local criterion for condensation at the center of the trap.

One can go beyond the semi-classical approximation and calculate numerically the central phase space density as a function of the total number of atoms. We consider as an example the trap parameters used in [18], where $\omega_x/(2\pi) = 9.4\,\mathrm{Hz}$ and $\omega_y/(2\pi) = 125\,\mathrm{Hz}$. In the typical case $k_B T/(\hbar\bar{\omega}) = 50$ ($T \simeq 80\,\mathrm{nK}$), the discrete summation of the Bose–Einstein occupation factors for $Z = 1$ gives $N_c \simeq 4800$ (the value obtained from the semi-classical result (3) is 4100). Using the expression for the energy eigenstates (Hermite functions), we also calculate the phase space density at the origin and we find $D(0) \simeq 13$. Let us emphasize that this value is a mere result of the finite size of the system, and does not have any character of universality.

3. Condensation of an ideal Bose gas in a harmonic + periodic potential

In order to produce a quasi 2D gas experimentally, one needs to freeze the motion along one direction of space, say z. In practice, this is conveniently done using the potential $V^{(\mathrm{lat})}(z) = V_0 \sin^2(kz)$ created by an optical lattice along this direction. A precise comparison between the measured critical atom number and the prediction for an ideal gas requires to properly model the confining potential and find its energy levels. This is the purpose of the present section.

3.1. The confining potential

The optical lattice is formed by two running laser waves of wavelength λ_L, propagating in the yz-plane with an angle $\pm\theta/2$ with respect to the y-axis. The period $\ell = \pi/k = \lambda_L/(2\sin(\theta/2))$ of the lattice along the z-direction can be adjusted to any value above $\lambda_L/2$ by a proper choice of the angle θ. For a blue-detuned lattice (λ_L is smaller than the atomic resonance wavelength), V_0 is positive and the atoms accumulate in the vicinity of the nodal planes $z = 0$ and $z = \pm\pi/k$,

etc. The oscillation frequency at the bottom of the lattice wells is $\omega_z^{(\mathrm{lat})} = 2\sqrt{V_0 E_r}/\hbar$, where $E_r = \hbar^2 k^2/(2m)$. In order for the quasi-2D regime to be reached, $\hbar\omega_z^{(\mathrm{lat})}$ must notably exceed the typical thermal energy $k_\mathrm{B}T$ as well as the interaction energy per particle for a non-ideal gas.

For a blue detuned lattice an additional confinement in the xy-plane must be added to the optical lattice potential. This is conveniently achieved using a magnetic trap, that creates a harmonic potential with frequencies ω_x and ω_y. The magnetic trap also provides an additional trapping potential $m\omega_z^2 z^2/2$ along the z-direction. The oscillation frequency ω_z created by the magnetic trap is usually much lower than the one created by the lattice $\omega_z^{(\mathrm{lat})}$. The main effect of the magnetic confinement along the z-direction is to localize the atoms in the $\mathcal{N}$ central lattice planes, where the effective number of planes $\mathcal{N} \sim 4\,k_\mathrm{B}T/(m\omega_z^2\ell^2)$. As we see below this number is on the order of 2–4 for the range of parameters explored in [18]. The fact that more than just one plane is populated is an important ingredient of the experimental procedure used in [17, 18]. It allows one to look for interferences between planes, and to access in this way the spatial coherence of the quasi-2D gas.

In order to extract thermodynamic information from the interference between planes, one must ensure that the various populated planes have the same temperature. This is achieved by using finite size lattice beams in the xy-plane, so that atoms in the high energy tail of the thermal distribution can actually travel quasi freely from one plane to the other, thus ensuring thermalization. In the experiments described in [17, 18], the waist W_x of the lattice beams along the x-direction was chosen accordingly. The total trapping potential can then be written in the following way

$$V(\mathbf{r}) = V^{(\mathrm{mag})}(\mathbf{r}) + V^{(\mathrm{lat})}(\mathbf{r}) \tag{5}$$

with

$$V^{(\mathrm{mag})}(\mathbf{r}) = \tfrac{1}{2}m\left(\omega_x^2 x^2 + \omega_y^2 y^2 + \omega_z^2 z^2\right), \tag{6}$$

$$V^{(\mathrm{lat})}(\mathbf{r}) = V_0\, \mathrm{e}^{-2x^2/W_x^2}\, \sin^2(k(z - z_0)). \tag{7}$$

Note that we have included here the offset z_0 between the optical lattice and the bottom of the magnetic potential; this quantity was not set to a fixed value in the experiments [17, 18]. We consider below two limiting situations: (i) $kz_0 = \pi/2$, with two principal equivalent minima at $kz = \pm\pi/2$; (ii) $kz_0 = 0$, with one principal minimum at $z = 0$ and two side minima at $kz = \pm\pi$. At very low temperatures, we expect that A will lead to two equally populated planes whereas configuration B will lead to one populated plane. For the temperature range considered in practice, the differences between the predictions for A and B are minor, as we will see below.

3.2. Renormalization of the trapping frequency ω_x by the optical lattice

In order to use the Bose–Einstein statistics for an ideal gas, one needs to know the position of the single particle energy levels. For the potential (5) it is not possible to find an exact analytical expression of these levels. However, if the extension of the atomic motion along the x-direction is smaller than the laser waist, an approximate expression can be readily obtained, as we show now.

The frequencies of the magnetic trap used in [17, 18] are $\omega_x = 2\pi \times 10.6\,\mathrm{Hz}$ and $\omega_y = \omega_z = 2\pi \times 125\,\mathrm{Hz}$. The optical lattice has a period $\pi/k = 3\,\mu\mathrm{m}$ ($E_r = \hbar^2k^2/(2m) = h \times 80\,\mathrm{Hz}$) and a potential height at center $U_0/h = 35\,\mathrm{kHz}$ ($1.7\,\mu\mathrm{K}$). The lattice oscillation frequency at center ($x = 0$) is thus $\omega_z^{(\mathrm{lat})}(x = 0) = 2\pi \times 3\,\mathrm{kHz}$ ($\hbar\omega_z^{(\mathrm{lat})}/k_\mathrm{B} = 150\,\mathrm{nK}$). When the atoms

occupy the ground state of the z-motion, they acquire the zero-point energy $\hbar\omega_z^{(\mathrm{lat})}(x)/2$ from the z-degree of freedom. The dependance on x of $\omega_z^{(\mathrm{lat})}(x)$, due to the Gaussian term $\mathrm{e}^{-2x^2/{W_x}^2}$ in the laser intensity, causes a renormalization of the x-frequency:

$$\omega_x^2 \to \omega'^2_x = \omega_x^2 - \frac{2\sqrt{V_0 E_r}}{m W_x^2}\,. \tag{8}$$

The waist of the lattice beams is $W_x = 120\,\mu$m which leads to $\omega'_x = 2\pi \times 9.4\,$Hz. A similar effect should in principle be taken into account for the frequency ω_y. However the scale of variation of the laser intensity along the y-axis is the Rayleigh length, which is much larger than the waist W_x, and the effect is negligible.

This simple way of accounting for the finiteness of the waist W_x is valid when the extension of the motion along x is small compared to W_x. For $T = 100\,$nK, the width of the thermal distribution along x is $\sqrt{k_\mathrm{B}T/m\omega_x^2} \sim 50\,\mu$m, which is indeed notably smaller than W_x. Taking into account the finiteness of W_x by a mere reduction of the trapping frequency along x is therefore valid for the major part of the energy distribution.

We note however that atoms in the high energy tail of the distribution ($E > 5\,k_\mathrm{B}T$ for our largest temperatures) can explore the region $|x| > W_x$, where the influence of the lattice beams is strongly reduced. In this region, the atoms can move from one lattice plane to the other. As explained above these atoms play an important role by ensuring full thermalization between the various planes. We now turn to an accurate treatment of the critical atom number required for Bose–Einstein condensation, taking into account these high energy levels for which the 2D approximation is not valid.

3.3. The critical atom number in a 'Born–Oppenheimer' type approximation

In order to get the single particle energy eigenstates in the lattice+harmonic potential confinement, and thus the critical atom number, one could perform a numerical diagonalization of the 3D Hamiltonian with the potential (5). This is however a computationally involved task and it is preferable to take advantage of the well-separated energy scales in the problem.

We first note that the trapping potential (5) is the sum of a term involving the variables x and z, and a quadratic component in y. The motion along the y-axis can then be separated from the xz problem, and it is easily taken into account thanks to its harmonic character. For treating the xz problem we use a 'Born–Oppenheimer' type approximation. We exploit the fact that the characteristic frequencies of the z-motion are at any point x notably larger than the frequency of the x-motion. This is of course true inside the lattice laser waist, since $\omega_z^{(\mathrm{lat})}/\omega_x \sim 300$, and it is also true outside the laser waist as the x-direction corresponds to the weak axis of our magnetic trap. Therefore we can proceed in two steps:

1. For any fixed x, we numerically find the eigenvalues $E_j(x)$, $j = 0, 1, \ldots$, of the z-motion in the $(V^{(\mathrm{mag})} + V^{(\mathrm{lat})})(x, z)$ potential. We determine the E_js up to the threshold $6\,k_\mathrm{B}T$ above which the thermal excitation of the levels is negligible. The result of this diagonalization is shown in figure 1 for the configurations A and B.
2. We then treat semi-classically the x motion on the various potential curves $E_j(x)$. Adding the result for the independent harmonic y-motion—also treated semi-classically—we obtain the surface density $n(x, y)$ (integral of the spatial density $n_3(\mathbf{r})$ along the

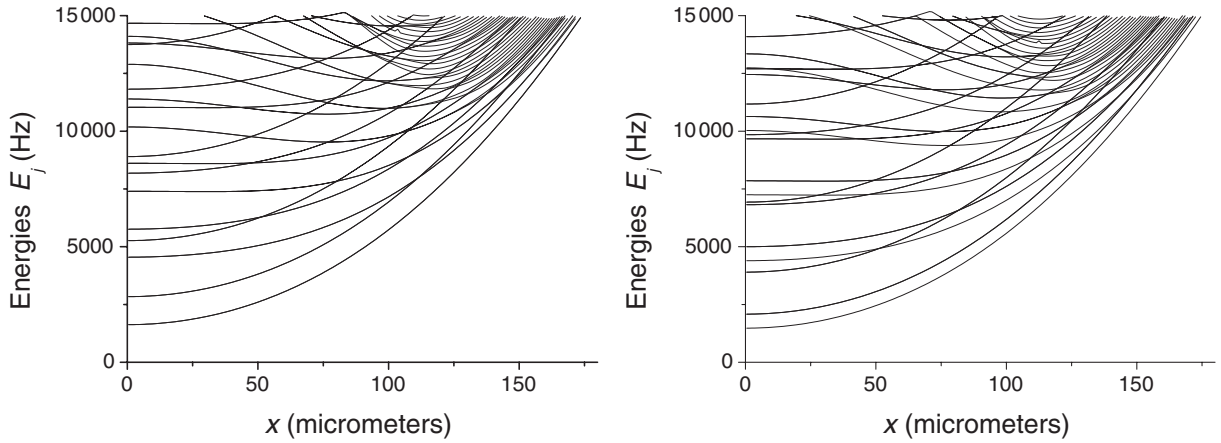

Figure 1. Eigenvalues of the z motion in the magnetic+optical x–z-potential, for fixed values of the x-coordinate (left: configuration A and right: configuration B).

direction z)

$$n(x, y) = \frac{1}{\lambda^2} \sum_j g_1 \left(Z \mathrm{e}^{-\beta(E_j(x)+V^{(\mathrm{mag})}(y))} \right). \tag{9}$$

This procedure yields a result that is identical to the semi-classical prediction in two limiting cases:

1. The pure 2D case, that is recovered for large waists and low temperatures. In this case the restriction to the closest-to-center lattice plane and to the first z-level is legitimate, and the sum over j contains only one significant term corresponding to (4).
2. The pure 3D harmonic case with zero lattice intensity where $E_j(x) = m\omega_x^2 x^2/2 + (j + 1/2)\hbar\omega_z$. In this case the sum over j in (9) leads to $n(x, y)\,\lambda^2 = g_2(Z\mathrm{e}^{-\beta V^{(\mathrm{mag})}(x,y)})/(\beta\hbar\omega_z)$, which coincides with the 3D result $D^{(3\mathrm{D})}(\mathbf{r}) = g_{3/2}(Z\mathrm{e}^{-\beta V(r)})$ when integrated along z.

Of course this procedure also allows to interpolate between these two limiting cases, which is the desired outcome. The integral of n in the xy-plane for $\mu = \min(E_j(x) + V^{(\mathrm{mag})}(y))$ gives the critical atom number $N_{\mathrm{c}}^{(\mathrm{lat,id})}(T)$ in the ideal gas model for this lattice geometry. It is shown in figure 2(a) for the two configurations A and B.

The critical atom number $N_{\mathrm{c}}^{(\mathrm{lat,id})}$ can be compared with the result for a single plane $N_{\mathrm{c}}^{(\mathrm{id})}$ with eigenfrequencies ω_x' and ω_y. The ratio gives the effective number of planes $\mathcal{N}_{\mathrm{eff}}$, shown as a function of temperature in figure 2(b) for the two configurations A and B. This ratio increases with temperature, which means that $N_{\mathrm{c}}^{(\mathrm{lat,id})}$ increases faster than T^2 with temperature in the temperature domain considered here. For example, in the range 50–110 nK, the variation of $N_{\mathrm{c}}^{(\mathrm{lat,id})}$ is well represented by T^β, with $\beta = 2.8$.

Three phenomena contribute significantly to this 'faster than T^2' increase of $N_{\mathrm{c}}^{(\mathrm{lat,id})}$. Firstly, in the lattice + harmonic potential geometry, the number of contributing planes increases with temperature, even if the atomic motion in each plane remains 2D (i.e. the atom number per plane increasing strictly as T^2). Secondly, we are exploring here a region of temperature where $k_{\mathrm{B}}T$ becomes non negligible with respect to $\hbar\omega_z^{(\mathrm{lat})}$ (the two quantities are equal for $T = 150$ nK), and the thermal excitations of the z motion in each lattice plane cannot be fully

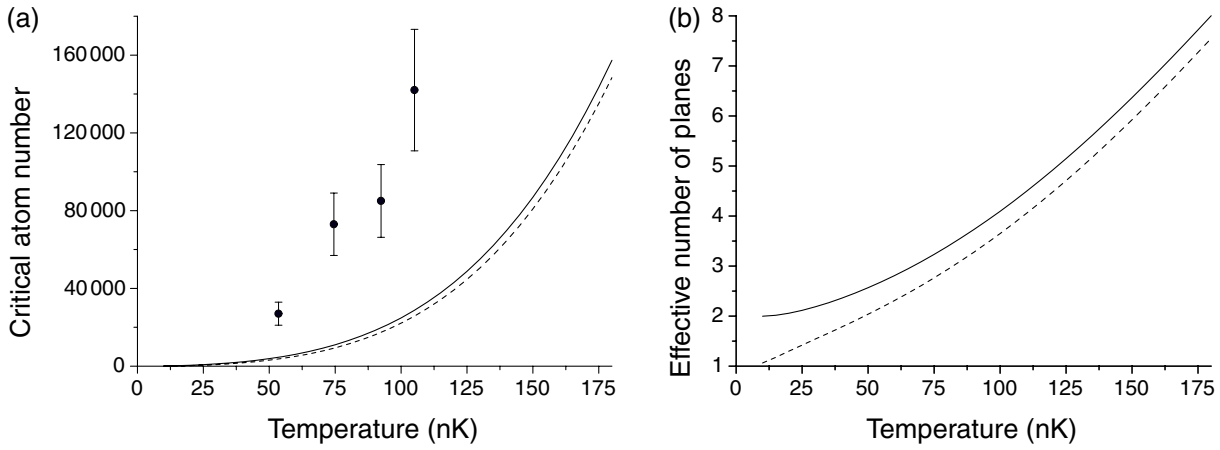

Figure 2. (a) Critical atom number $N_c^{(\mathrm{lat,id})}$ in the ideal gas model for the optical lattice + magnetic trap configuration, as a function of temperature. The points represent the experimental results of [18], and the error bars combine the systematic and statistical uncertainties on atom numbers. (b) Effective number of planes $\mathcal{N}_{\mathrm{eff}} = N_c^{(\mathrm{lat,id})}/N_c^{(\mathrm{id})}$ as a function of temperature. In both panels the continuous (dashed) line is for configuration A (B). The calculation is performed using the first 100 eigenvalues of the z-motion, and the first neglected levels $E_j(x)$ are 22 kHz (1 μK) above the bottom of the trap.

neglected. Thirdly, for the largest considered temperatures, the extension of the atomic motion along x becomes comparable to the laser waist, and the lattice strength is then significantly reduced.

3.4. Comparison with experimental results

In [18] the critical atom number in the lattice + magnetic trap configuration was measured for various 'effective' temperatures, deduced from the width of the quasi-Gaussian atomic distribution. Each critical point $(N_c^{(\mathrm{exp})}, T_c^{(\mathrm{exp})})$ was defined as the place where a bimodal spatial distribution appeared, if the atom number was increased beyond this point at constant temperature, or the temperature reduced at constant atom number. The critical point also corresponded to the threshold for the appearance of interferences with a significant contrast between adjacent planes. The experimental measurements of critical points, taken over the effective temperature range 50–110 nK, are shown as dots in figure 2(a). The systematic + statistical uncertainty of the atom number calibration is 25%. Assuming that the effective temperatures coincide with the true ones (this point will be examined in section 4.6) we find $N_c^{(\mathrm{exp})}/N_c^{(\mathrm{lat,id})} \sim 5.3\ (\pm 1.2)$.

In addition to this large discrepancy between experiment and ideal gas model for the critical atom numbers, one also finds a strong mismatch concerning the functional shape of the column density $\int n(x, y)\,\mathrm{d}y$ that was measured in absorption imaging in [17, 18]. While the experimental result is quasi-Gaussian, the column density profiles calculated for an ideal gas at the critical point are much 'peakier'. An example is given in the appendix for a single plane, and we checked that a similar shape remains valid for our harmonic + lattice potential.

We, therefore, conclude that the experimental results of [18] cannot be accounted for with this ideal gas prediction for 'conventional' BEC.

4. Interactions in a quasi 2D trapped Bose gas

To improve the agreement between the experimental results and the theoretical modeling we now take repulsive atomic interactions into account. In a first stage we present a 2D MF analysis, in which the motion along z is assumed to be completely frozen whereas the xy motion is treated semi-classically. In order to model interactions in this case, we start from the 3D interaction energy $(g^{(3D)}/2)\int n_3^2(\mathbf{r})\,\mathrm{d}^3r$, where $g^{(3D)} = 4\pi\hbar^2 a/m$ and a is the scattering length. The z-degree of freedom is restricted to the Gaussian ground state of the confining potential, with an extension $a_z = \sqrt{\hbar/(m\omega_z^{(\mathrm{lat})})}$, and the interaction energy is

$$E_{\mathrm{int}} = \frac{g}{2}\int n^2(\mathbf{r})\,\mathrm{d}^2r\ .$$

We set $g = \hbar^2\tilde{g}/m$, where the dimensionless parameter $\tilde{g} = \sqrt{8\pi}\,a/a_z$ characterizes the strength of the 2D interaction (for a more elaborate treatment of atomic interactions in a quasi-2D geometry, see [25, 26]). For the optical lattice used in [18], we find $\tilde{g} = 0.13$. In a second stage, we take into account the residual excitation of the z motion in a 'hybrid' 3D MF approximation. We calculate in a self-consistent way the quantum levels of the z-motion, whereas the motion in the xy-plane is still treated semi-classically.

4.1. Criticality within MF solutions: 3D versus 2D

We start our discussion with a brief reminder of the role of (weak) interactions in a trapped 3D Bose gas [27]. One often uses the MF Hartree–Fock approximation, that gives in particular a relatively accurate value for the shift of the critical temperature for Bose–Einstein condensation. In order to calculate this shift, one assumes that above the critical temperature, the atoms evolve in the effective potential $V_{\mathrm{eff}}(\mathbf{r}) = V(\mathbf{r}) + 2g^{(3D)}n_3(\mathbf{r})$. The phase space density in $\mathbf{r}$ is thus a solution of $D^{(3D)}(\mathbf{r}) = g_{3/2}(Z\mathrm{e}^{-\beta V_{\mathrm{eff}}(\mathbf{r})})$. As for the ideal case this equation ceases to have a solution when the central phase space density goes above $g_{3/2}(1)$. The mere effect of repulsive interactions within the MF approximation is to increase the number of atoms for which this threshold is met. The increase is typically $\sim$10% for standard trap and interaction parameters [27].

For a trapped 2D gas this treatment based on a local criterion (phase space density at center) cannot be used. Indeed as explained in section 2.2, it is not possible to identify a critical phase space density at which BEC of the 2D gas is expected. On the contrary the semiclassical approximation leads to an infinite central density at the critical point, and it is unclear whether one can achieve an arbitrarily large spatial density in the presence of repulsive interactions.

One could also look for a global criterion for criticality based on the total atom number. The starting point is the solution of the MF equation

$$D(\mathbf{r}) = g_1\left(Z\mathrm{e}^{-\beta V_{\mathrm{eff}}(\mathbf{r})}\right) \tag{10}$$

with $V_{\mathrm{eff}}(\mathbf{r}) = V(\mathbf{r}) + 2gn(\mathbf{r})$. When $g = 0$, we saw in section 2 that the solution of (10) can only accommodate a finite number of atoms (3). However the situation is dramatically changed

in the presence of repulsive interactions. Indeed for any nonzero g, a solution to (10) exists for arbitrarily large atom numbers [28]. Consequently no critical point can be found by simply searching for a maximal atom number compatible with (10). In the following we will therefore turn to a different approach, starting from the known exact (i.e. non-MF) results concerning the critical BKT point in a uniform interacting 2D Bose gas. The MF approximation will be used in a second stage, in combination with the local density approximation (LDA), to determine the critical atom number in the trapped system.

Note that it is also possible to pursue the search for a critical point only within the MF approach, by looking for example whether its solution exhibits a thermodynamical or dynamical instability above a critical atom number [29, 30]. This instability would be an indication that the system tends to evolve towards a different kind of state, with a non-zero quasi-condensed and/or superfluid component, and quasi-long range order [31, 32].

4.2. The BKT transition and the LDA

In an infinite uniform 2D Bose fluid, repulsive interactions have a dramatic effect since they can induce a transition from the normal to the superfluid state, when the temperature is lowered below a critical value. The superfluid density jumps from 0 to $4/\lambda^2$ at the transition point [33]. The microscopic mechanism of the 2D superfluid transition has been elucidated by BKT. For a temperature larger than the critical temperature, free vortices proliferate in the gas, destroying the superfluidity. Below the transition, vortices exist only in the form of bound pairs involving two vortices of opposite circulations, which have little influence on the superfluid properties of the system.

In a uniform system the phase space density D is a function of the chemical potential and temperature $D = F(\mu, T)$. For any given T, the superfluid transition occurs when μ is equal to a critical value $\mu_c(T)$. The corresponding critical value D_c for the phase space density depends on the interaction strength as [34]–[36]

$$D_c = \ln(\xi/\tilde{g}), \tag{11}$$

where ξ is a dimensionless number. A recent Monte Carlo analysis provided the result $\xi = 380 \pm 3$ [23] (see also [37]). For $\tilde{g} = 0.13$ this gives a critical phase space density $D_c = 8.0$.

We now consider a trapped gas whose size is large enough to be well described by the LDA. The phase space density in $\mathbf{r}$ is given by $D(\mathbf{r}) = F(\mu - V(\mathbf{r}), T)$ and a superfluid component forms around the center of the trap if the central phase density $D(0)$ is larger than D_c [38]. The edge of the superfluid region corresponds to the critical line where $\mu - V(\mathbf{r}) = \mu_c$. The phase space density along this line is equal to D_c, independently of the total number of atoms in the trap. This can be checked experimentally and constitutes a validation of the LDA. The integration of the experimental data along the line of sight y does not lead to any complication because the trapping potential is separable, $V(\mathbf{r}) = V_1(x) + V_2(y)$. Therefore the edges of the superfluid region along the x-axis are located in $\pm x_c$ such that $V_1(x_c) = \mu - \mu_c$ (see figure 3(a)), and the column density along the line of sight passing in $x = x_c$ is

$$n_{col}(x_c) = \frac{1}{\lambda^2}\int D(x_c, y)\,\mathrm{d}y = \frac{1}{\lambda^2}\int F(\mu_c - V_2(y), T)\,\mathrm{d}y \tag{12}$$

which is also independent of the total atom number N. This is confirmed experimentally, as shown in figure 3(b) where we plot $n_{col}(x_c)$ as a function of N. The slight increase (10%) of

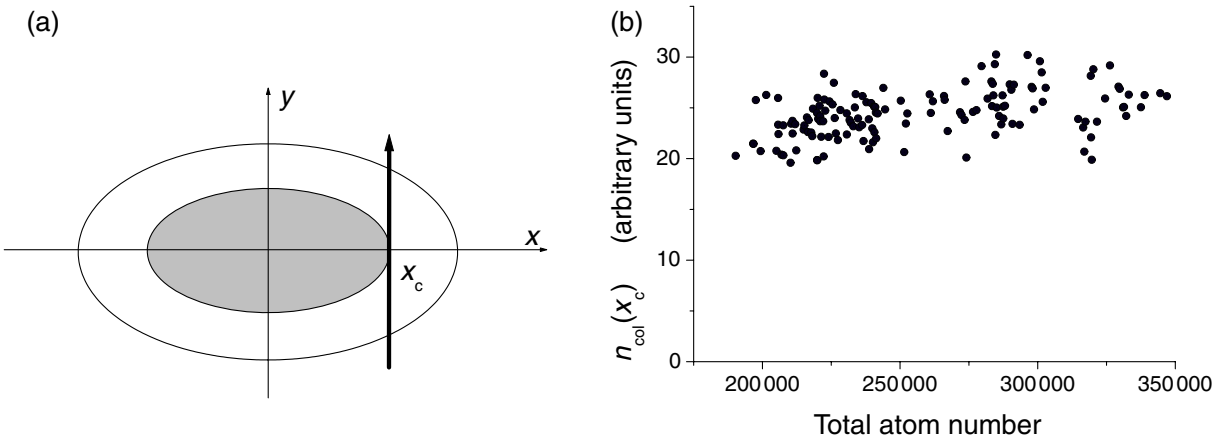

Figure 3. Check of the LDA. (a) The column density $n_{\rm col}$ is measured at the edge $x = x_{\rm c}$ of the central part (in gray) of the bimodal distribution. (b) $n_{\rm col}(x_{\rm c})$ is plotted as a function of the total atom number N in the harmonic trap + lattice configuration. Within the LDA for a single plane, $n_{\rm col}(x_{\rm c})$ should be independent of N, which is indeed nearly the case. The small variation of $n_{\rm col}(x_{\rm c})$ for large N may be due to the appearance of a nonnegligible population in side planes of the optical lattice potential. The data have been taken for the effective temperature $T = 105\,{\rm nK}$. Each point is extracted from a single image.

$n_{\rm col}(x_{\rm c})$ for atom numbers larger than 3×10^5 may be due to the fact that the population of additional planes becomes non-negligible for such large N.

The possibility to use the LDA to study the BKT critical point in a harmonically trapped quasi-2D Bose gas has been checked recently by Holzmann and Krauth using a QMC analysis [24]. For trap parameters close to the ones of [18] they have shown that a superfluid component, characterized by a reduced moment of inertia, indeed appears at the center of the trap when the local phase space density reaches a critical value close to the prediction (11).

4.3. Density profile in the 2D MF theory

In this section, we use the MF Hartree–Fock approximation (10) to calculate the density profile of the trapped atomic cloud. As we mentioned above, this equation admits a solution for any value of the fugacity Z, and therefore for an arbitrarily large number of particles. Rewriting (10) as

$$D(\mathbf{r}) = -\ln\left(1 - Z{\rm e}^{-\tilde{g}D(\mathbf{r})/\pi}{\rm e}^{-\beta V(\mathbf{r})}\right) \tag{13}$$

we see that the value of D for any temperature and at any point in space depends only on the parameter R defined by $R^2 = (x/x_T)^2 + (y/y_T)^2$, where $x_T = (\omega_x^2 m\beta)^{-1/2}$ and $y_T = (\omega_y^2 m\beta)^{-1/2}$. The total atom number is given by

$$N = \left(\frac{k_{\rm B}T}{\hbar\bar{\omega}}\right)^2 \int_0^\infty \tilde{D}(R) R\,{\rm d}R, \tag{14}$$

where $\tilde{D}(R)$ is the solution of the reduced equation

$$\tilde{D}(R) = -\ln\left(1 - Z{\rm e}^{-\tilde{g}\tilde{D}(R)/\pi}{\rm e}^{-R^2/2}\right). \tag{15}$$

Quite remarkably this result for $\tilde{D}(R)$ neither depends on the trap parameters, nor on the temperature. The only relevant parameters are the fugacity Z and the reduced interaction strength $\tilde{g}$. The scaling of the atom number N with the temperature and the trap frequency in (14) is therefore very simple. In particular it does not depend on the trap anisotropy ω_y/ω_x but only on the geometric mean $\bar{\omega}$.

For atom numbers much larger than $N_c^{(id)}$ it is interesting to note that the radial density profile deduced from the MF equation (13) exhibits a clear bi-modal shape, with wings given by $n(r)\lambda^2 \simeq Ze^{-\beta V(\mathbf{r})}$ and a central core with a Thomas–Fermi profile $2gn(r) \simeq \mu - V(\mathbf{r})$. However, this prediction of a bi-modal distribution using the Hartree–Fock approximation cannot be quantitatively correct. Indeed the Hartree–Fock treatment assumes a MF energy $2gn$. The factor 2 in front of this energy originates from the hypothesis that density fluctuations are those of a Gaussian field $\langle n^2\rangle = 2\langle n\rangle^2$. Actually when the phase space density becomes significantly larger than 1, density fluctuations are reduced and one approaches a situation closer to a quasi-condensate in which $\langle n^2\rangle \sim \langle n\rangle^2$ [23]. Taking into account this reduction could be done for example using the equation of state obtained from a classical field Monte Carlo analysis in [39].

4.4. Critical atom number in the 2D MF approach

We now use the solution of the MF equation (13) to evaluate the critical atom number $N_c^{(mf)}$ that is needed to reach the threshold (11) for the BKT transition at the center of the trap $D(0) = \ln(\xi/\tilde{g})$. For a given interaction strength $\tilde{g}$ we vary the fugacity Z and solve numerically (13) at any point in space. Examples of spatial density profiles at the critical point are given in the appendix, both before and after time-of-flight. The integration of the density profile over the whole xy-plane gives the total atom number N. From (14) and (15), it is clear that the scaling of $N_c^{(mf)}$ with the frequencies $\omega_{x,y}$ and with the temperature is identical to the one expected for an ideal trapped gas.

We have plotted in figure 4(a) the variation of $D(0)$ as a function of $N/N_c^{(id)}$ for various interaction strengths. For a given atom number the phase space density at the center decreases when the strength of the interactions increases, as expected. The numerical result for $N_c^{(mf)}$ is plotted as a dashed line in figure 4(a). We find that it is in excellent agreement—to better than 1%—with the result of [38]

$$\frac{N_c^{(mf)}}{N_c^{(id)}} = 1 + \frac{3\tilde{g}}{\pi^3} D_c^2, \tag{16}$$

over the whole range $\tilde{g} = 0$–1. This analytical result was initially derived in [38] for $g \ll 1$ using an expansion around the solution for the ideal Bose gas, but this approximation can actually be extended to an arbitrary value of $\tilde{g}$ [40]. The strongly interacting limit ($3\tilde{g}D_c^2/\pi^3 > 1$) can be easily understood by noticing that in this case, the atomic distribution (10) nearly coincides with the Thomas–Fermi profile $2gn(r) = \mu - V(r)$. Using the relation between the total atom number and the central density for this Thomas–Fermi distribution $N = 2\pi\tilde{g}(n(0)a_{ho}^2)^2$ (with $a_{ho} = (\hbar/(m\omega))^{1/2}$), one then recovers the second term of the right-hand side of (16).

Let us emphasize that figure 4(a) is a mix of two approaches: (i) the MF model, that does not lead in itself to a singularity along the dashed line of figure 4(a). (ii) The BKT theory for a uniform system, which is beyond a MF treatment and which has been adapted to the trapped case using the LDA in order to obtain the critical number indicated by the dashed line.

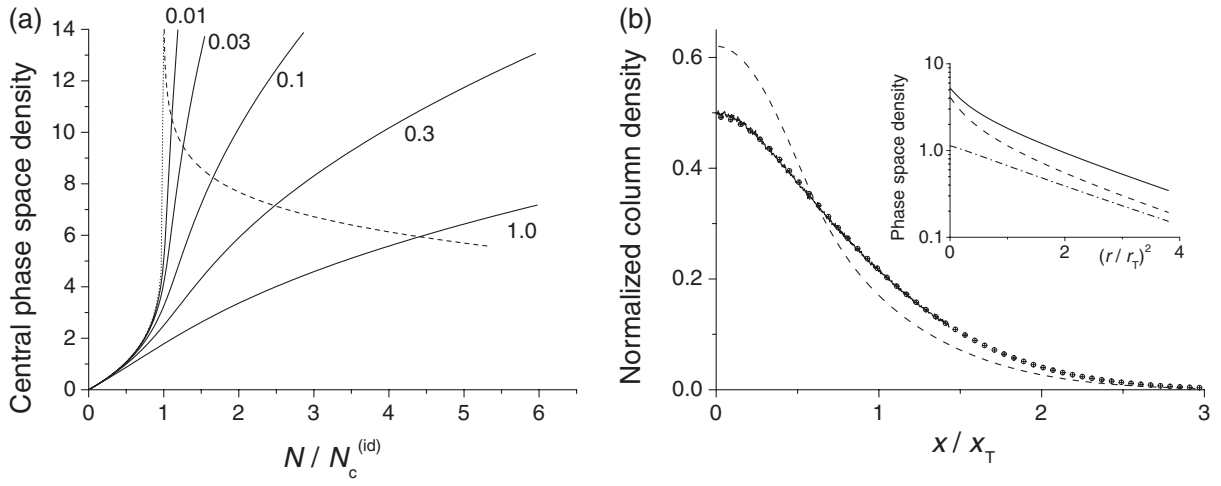

Figure 4. (a) Central phase space density predicted by the 2D MF theory, as a function of the atom number for various interaction strengths $\tilde{g}$. The dotted line represents the semi-classical prediction for the ideal gas. The dashed line indicates where the threshold for superfluidity (11) is met at the center of the trap. (b) Column density for $N = N_c^{(mf)} = 36\,000$ atoms in an isotropic trap ($\omega_x = \omega_y = \omega$, $\tilde{g} = 0.13$, $k_B T = 110\,\omega$). The dashed line is the result of the 2D MF analysis of section 4.3. The continuous line is the 3D QMC result obtained in [24], with $\omega_z = 83\omega$ and $a = \tilde{g} a_z/\sqrt{8\pi}$. The dots are the result of the hybrid 3D MF calculation of section 4.5 for the same parameters. Inset: Prediction of the hybrid 3D MF approach for the phase space density (log scale) as a function of r^2 (a Gaussian distribution leads to a straight line). Continuous line: total phase space density; dashed line: phase space density associated with the ground state φ_1 of the z-motion; dash-dotted line: phase space density associated with all other states φ_j, $j \geqslant 2$.

We now compare the 2D MF prediction with the results of the QMC calculation of [24], looking first at the critical atom number and then at the density profiles. For $\tilde{g} = 0.13$ the MF prediction for the critical number (16) is $N_c^{(mf)}/N_c^{(id)} = 1.8$. This is in relatively good agreement with the QMC calculation of [24], which gives $T_c^{(QMC)} = 0.70\, T_c^{(id)}$ or equivalently $N_c^{(QMC)}/N_c^{(id)} = 2.0$. The QMC calculation has been performed for various atom numbers N, for a 3D harmonic trap such that $\omega_z/\omega = 0.43\sqrt{N}$ and a 3D scattering length $a = \tilde{g} a_z/\sqrt{8\pi}$, with $\tilde{g} = 0.13$.

The agreement between the 2D MF and the QMC approaches is not as good for the density profiles close to the critical point. An example is shown in figure 4(b), where we take $k_B T = 110\,\hbar\omega$ ($N_c^{(id)} = 20\,000$). We choose $N = N_c^{(mf)} = 36\,000$ and we plot the column density $n_{col}(x)$ obtained by integrating the spatial density along the directions y and z. The MF result is shown as a dashed line, and it notably differs from the QMC result, plotted as a continuous line. As we show below this disagreement is essentially a consequence of the residual excitation of the z-motion ($k_B T/(\hbar\omega_z) = 1.4$), that is neglected in the 2D MF approach, whereas it is implicitly taken into account in the 3D QMC calculation.

4.5. The hybrid 3D MF approach

In this section, we extend the 2D MF treatment to take into account the residual excitation of the z-motion. As pointed out to us by the authors of [24], this is necessary for a quantitative analysis of the experiment [18], since the temperature and the chemical potential at the critical point were not very small compared to $\hbar\omega_z^{(\mathrm{lat})}$, but rather comparable to it.

We follow here a method related to the one developed in section 3 to analyze the ideal gas case. We start from a trial 3D density distribution $n_3(\mathbf{r})$. At any point (x, y), we treat the z-motion quantum mechanically and solve the eigenvalue problem for the z-variable

$$\left[\frac{-\hbar^2}{2m}\frac{\mathrm{d}^2}{\mathrm{d}z^2} + V_{\mathrm{eff}}(\mathbf{r})\right]\varphi_j(z|x,y) = E_j(x,y)\,\varphi_j(z|x,y), \tag{17}$$

where $V_{\mathrm{eff}}(\mathbf{r}) = m(\omega_x^2x^2 + \omega_y^2y^2 + \omega_z^2z^2)/2 + 2g^{(3\mathrm{D})}n_3(\mathbf{r})$ and $\int|\varphi_j(z|x,y)|^2\,\mathrm{d}z = 1$. Treating the xy-degrees of freedom semi-classically, we obtain a new spatial density

$$n_3'(\mathbf{r}) = -\frac{1}{\lambda^2}\sum_j|\varphi_j(z|x,y)|^2\ln\left(1-\mathrm{e}^{\beta(\mu-E_j(x,y))}\right). \tag{18}$$

We then iterate this calculation until the spatial density $n_3(\mathbf{r})$ reaches a fixed point [41]. With this method, we fulfill two goals. (i) We take into account the residual thermal excitation of the levels in the z-direction. (ii) Even at zero temperature we take into account the deformation of the z-ground state due to interactions.

This 'hybrid 3D MF' method is different from the standard MF treatment used to describe 3D Bose gases. In the latter case, all three degrees of freedom are treated semi-classically, which is valid when the particle population is distributed smoothly over several quantum states. This standard 3D MF would not be applicable in our case, where a significant part of the total population accumulates in the lowest state φ_1.

An example is shown in figure 4(b), where we plot the column density $n_{\mathrm{col}}(x)$ obtained with this hybrid MF method, taking into account the first 5 eigenstates φ_j. The agreement between the hybrid 3D MF prediction and the 'exact' QMC prediction of [24] is excellent. This shows that the predictions of this hybrid 3D MF approach are reliable as long as the superfluid transition has not been reached at the center of the trap.

We show in the inset the variations of the phase space density $D(r)$. We plot $\ln(D)$ as a function of r^2, so that a Gaussian distribution would appear as a straight line. The dashed line is the phase-space density associated with the ground state of the z motion φ_1, and the dash-dotted line corresponds to the excited states φ_j, $j \geqslant 2$. The continuous line is the total phase-space density. At the center of the trap, as a consequence of Bose statistics, most of the population (80%) accumulates in the ground state φ_1. For $r \geqslant r_T$, the repartition of the population among the eigenstates of the z motion follows the Boltzmann law, and ∼50% of the atoms occupy the excited states φ_j, $j \geqslant 2$. A practical consequence of this increasing influence of excited states of the z motion with increasing r is that the total phase space density profile is notably closer to a Gaussian distribution than when only the ground state of the z motion is retained in the calculation, as is the case in the 2D MF approach.

Finally we mention that we have also developed a simpler version of this hybrid 3D MF analysis, in which the φ_j levels are not calculated self-consistently, but are assumed to coincide with the energy eigenstates in the potential $m\omega_z^2z^2/2$ (see also [42]). For the domain of parameters relevant for the experiment, the two approaches lead to very similar results.

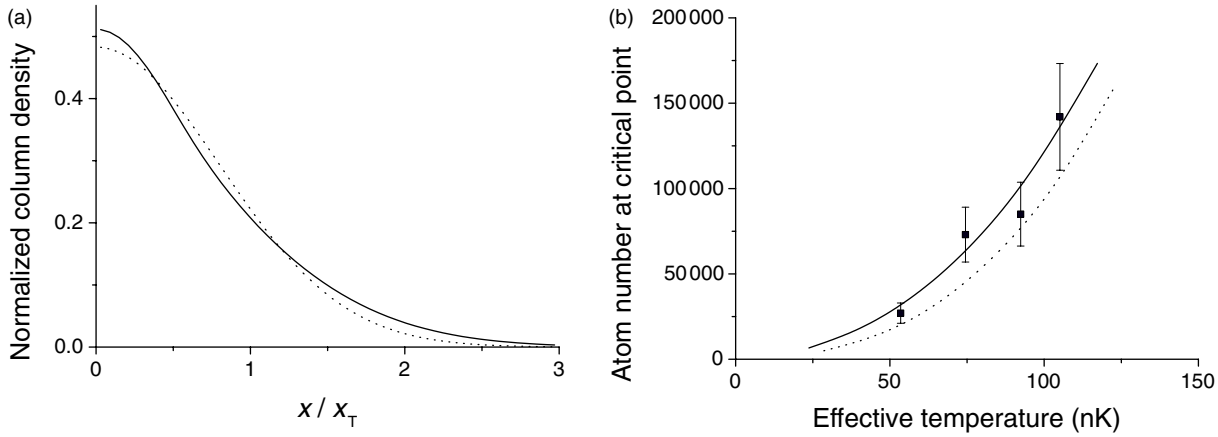

Figure 5. (a) Hybrid 3D MF prediction for the normalized column density for the lattice configuration A, $T = 150\,\mathrm{nK}$ and $N = 110\,000$ atoms. For these parameters the phase space density associated with the lowest eigenvalue of the z motion reaches the critical value D_c at the center of the most populated planes. The dotted line is a Gaussian fit which gives the effective temperature $T_{\mathrm{eff}} = 0.64\,T = 96\,\mathrm{nK}$. (b) Critical atom number as a function of the effective temperature obtained from a Gaussian fit of the MF result. The continuous line (resp. dashed line) is for configuration A (resp. B). The points are the experimental results of [18], already shown in figure 2.

4.6. MF approach for the lattice configuration and comparison with experiment

In order to compare the predictions of the MF approach with the experimental results, we now turn to the lattice geometry, corresponding to a stack of parallel planes located in $z_j = z_0 + j\ell$, j integer. For simplicity we assume that the laser waist W_x is large compared to the spatial extent of the atomic cloud, so that we can treat the gas as a superposition of independent harmonically trapped systems. Each system is located in the vicinity of a nodal plane of the optical lattice, and is treated as a harmonic trap with frequencies ω'_x, ω_y and $\omega_z^{(\mathrm{lat})}$. Note that we include here 'by hand' the renormalization $\omega_x \to \omega'_x$ of the x-frequency due to the finiteness of the laser waist, that we discussed in section 3.2. The magnetic trap adds an extra confinement along the z-axis with a frequency ω_z so that the chemical potential for the plane z_j is $\mu_j = \mu - m\omega_z^2(z_0 + j\ell)^2/2$. We assume that the critical point is reached when the phase space density associated with the lowest eigenstate φ_1 in the most populated plane reaches the critical value (11). Once the corresponding fugacity is determined, we calculate the spatial distribution in each plane, sum up the various contributions, and integrate the spatial distribution over the line of sight y to obtain the column density $n_{\mathrm{col}}(x)$.

A typical result for n_{col} is given in figure 5(a) for the temperature $T = 150\,\mathrm{nK}$ and for the lattice configuration A. The total atom number is 1.1×10^5. It is well fitted by a Gaussian distribution $\exp(-x^2/2x_0^2)$ (dotted line), so that we can assign an effective temperature to this distribution $T_{\mathrm{eff}} = m\omega_x^2 x_0^2/k_{\mathrm{B}}$. In the example of figure 5(a), we find $T_{\mathrm{eff}} = 0.64\,T$ (96 nK). For the same T and a lattice in configuration B, the effective temperature obtained with a Gaussian fit is $T_{\mathrm{eff}} = 0.69\,T$ (103 nK) and the total atom number is $N = 1.0 \times 10^5$. We have repeated this

procedure for temperatures T in the range 100–200 nK and consistently found the ratio $T_{\rm eff}/T$ in the range 0.6–0.7, with a quality of the Gaussian fit similar to what is shown in figure 5(a).

We have plotted in figure 5(b) the calculated total number of atoms in the lattice at the critical point, as a function of the effective temperature deduced from the Gaussian fit to the column density. We have also plotted the experimental points of [18] already shown in figure 2. We remind the reader that the experimental 'effective' temperature is also deduced from a Gaussian fit to the measured column density. One reaches in this way good agreement between the experimental results and the hybrid 3D MF prediction. The predicted density profiles with the 3D MF approach therefore provide a satisfactory means for temperature calibration. They indicate in particular that for the experiment [18], the effective temperatures are typically 30–40% below the real ones. To improve on the comparison between theory and experiment, a more controlled set-up will be needed with an accurate independent measurement of temperature, as well as the possibility of addressing only a single or a fixed number of planes.

5. Summary and concluding remarks

In this paper, we have analyzed the critical point of a trapped quasi-2D Bose gas. We have shown that the experimental results of [18] are not in agreement with the ideal Bose gas theory. The differences are found first at the qualitative level: the predicted shape for the ideal gas distribution is 'peaky' around its center, which clearly differs from the quasi-Gaussian measured profile. Also the measured critical atom numbers $N_{\rm c}(T)$ do not agree with the predictions for the ideal gas. Using the 'effective' temperatures obtained by treating the Gaussian profiles as Boltzmann distributions, the measured $N_{\rm c}(T)$ are larger by a factor $\sim$5 than the predicted ones. We then discussed the predictions of a hybrid approach based on the LDA. It combines the density profile calculated using a MF Hartree–Fock treatment, and the known result for the critical phase space density for the BKT transition in an infinite, uniform 2D Bose gas [23]. We compared the predictions of this approach with the results of a recent QMC calculation [24] and reached the following conclusions: (i) if one is interested only in the critical atom number, it is sufficient to use a strictly 2D MF approach. It leads to the approximate analytical result (16), in good agreement with the QMC prediction. For the experimental parameters of [18] the critical atom number is $N_{\rm c} \sim 2N_{\rm c}^{\rm (id)}$. (ii) In order to calculate accurately the density profiles for the experimental temperature range ($k_{\rm B}T$ between $0.5\,\hbar\omega_z$ and $\hbar\omega_z$), it is important to take into account the residual excitation of the z degree of freedom (the same conclusion has been reached in [42]). We have presented a hybrid 3D MF approximation which leads to density distributions in excellent agreement with the QMC predictions close to the critical point. When generalized to the lattice geometry used in the experiment, the predicted density profiles are close to a Gaussian distribution, and good agreement between theory and experiment is reached concerning the critical number $N_{\rm c}(T)$ when the predicted density profile is used for temperature calibration.

We now briefly discuss the nature of the critical point that appears in the trapped 2D Bose gas and compare it with 'standard' Bose–Einstein condensation. For a harmonically trapped ideal gas, we recall that conventional Bose–Einstein condensation is expected in the thermodynamic limit $N \to \infty$, $\omega \to 0$ and $N\omega^2$ constant. This is a consequence of the density of states for a quadratic Hamiltonian around the zero energy. The price to pay for this condensation in a 2D system is a diverging atomic density at the center of the trap. In contrast, when interactions are taken into account, the MF approximation leads to the potential $V(\mathbf{r}) + 2gn(\mathbf{r})$

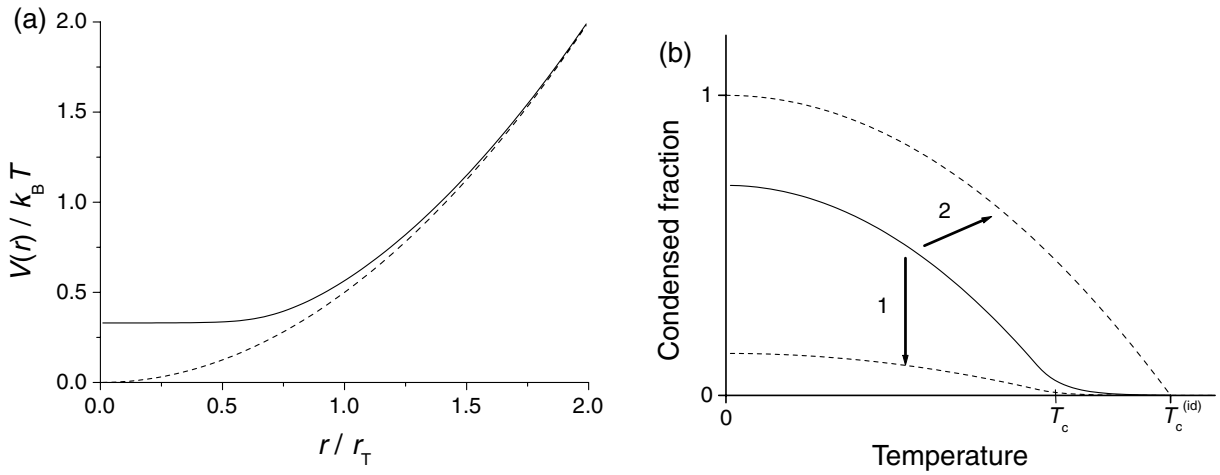

Figure 6. (a) Trapping potential $V(r)$ (dashed line) and effective MF potential $V_{\rm eff}(r) = V(r) + 2gn(r)$ (continuous line), for $\tilde{g} = 0.13$ and a central phase space density equal to the critical value (11). (b) Schematic representation of the condensed fraction in a finite 2D Bose gas for a given interaction strength $\tilde{g}$ (continuous line). Two limits can be considered: (1) thermodynamic limit $N \to \infty, \omega \to 0, N\omega^2$ constant; the condensed fraction tends to zero for any nonzero value of $\tilde{g}$, (2) ideal gas limit $\tilde{g} \to 0$.

that is flat at the origin (figure 6(a) and [38]). The 'benefit' of the harmonic trapping potential is lost and the physics of the trapped interacting gas is very similar to that of a uniform system. In particular one expects in the thermodynamic limit the appearance of quasi-long range order only, with no true Bose–Einstein condensate [25].[6] The transition between the ideal and the interacting case is explicit in equations (11) and (16), where the limit $\tilde{g} \to 0$ gives $D_{\rm c} \to +\infty$ and $N_{\rm c}^{\rm (mf)}/N_{\rm c}^{\rm (id)} \to 1$. In particular (16) can be used to separate a 'BEC-dominated' regime where $\eta = 3\tilde{g}D_{\rm c}^2/\pi^3 \ll 1$ and $N_{\rm c} \simeq N_{\rm c}^{\rm (id)}$, and a 'BKT-dominated' regime, where the contribution of η is dominant and $N_{\rm c} \gg N_{\rm c}^{\rm (id)}$. In the latter case, the spatial distribution in the MF approximation is a Thomas–Fermi disk with radius $R_{\rm TF}$ and (16) is equivalent (within a numerical factor) to the BKT threshold (11) for a uniform gas with density $n = N/(\pi R_{\rm TF}^2)$. The rubidium gas studied in [17, 18] is at the border of the 'BKT-dominated' regime ($\eta \simeq 1$), whereas previous experiments performed on quasi-2D gases of sodium atoms [8] corresponded to $\eta \sim 0.1$, well inside the 'BEC-dominated' regime.

Finally, we must take into account the finite size of the gas in our discussion. It is known from simulations of 2D spin assemblies that for a finite size system, the average magnetization increases rapidly around the BKT transition [43]. It is at first sight surprising that this magnetization can be used as a signature of BKT physics, since it would not exist in an infinite system where a genuine BKT transition takes place. However, it is relevant for all practical 2D situations: as emphasized in [43] one would need extremely large systems ('bigger than the state of Texas') to avoid a significant magnetization even just below the transition point. A similar phenomenon occurs for a finite size Bose gas. A few states acquire a large

[6] A similar flattening of the MF potential occurs in 3D, but it has no important consequence in this case since true BEC is possible in an infinite, uniform 3D system.

population around the transition point, and this allows for the observation of good contrast interferences between two independent gases. In particular the condensed fraction f_0 (largest eigenvalue of the one-body density matrix) is expected to grow rapidly at the critical point, and this has been quantitatively confirmed by the QMC calculation of [24]. To illustrate this point we have schematically plotted in figure 6(b) the expected variations of f_0 with the parameters of the problem. For given $\tilde{g}$ and N, f_0 takes significant values for $T < T_c$ (continuous line). If the strength of the interactions $\tilde{g}$ is kept constant, the condensed fraction f_0 tends to zero for any finite temperature if the thermodynamic limit is taken (arrow 1 in figure 6(b)). Note that the superfluid fraction should tend to a finite value in this limiting procedure. Now one can also keep N constant and decrease $\tilde{g}$ to zero (arrow 2 in figure 6(b)). In this case one expects to recover the ideal gas result $f_0 = 1 - (T/T_c^{(\mathrm{id})})^2$ for any value of N. Therefore, we are facing here a situation where two limits do not commute: $\lim_{N\to\infty}\lim_{g\to 0} \neq \lim_{g\to 0}\lim_{N\to\infty}$. Of course this does not cause any problem in practice since none of these limits are reached. In this sense the phenomenon observed in our interacting, trapped 2D Bose gas is hybrid: the transition point is due to BKT physics (the density of states of the ideal 2D harmonic oscillator does not play a significant role because of the flattening of the potential), but thanks to the finite size of the system, some diagnoses of the transition such as the appearance of interferences, take benefit of the emergence of a significant condensed fraction.

Acknowledgments

We are indebted to Markus Holzmann and Werner Krauth for numerous discussions, for providing the quantum Monte Carlo data shown in figure 4 and for pointing out the significant role of the excitation of the z motion in our experiments. We also thank Yvan Castin and Pierre Cladé for helpful discussions. PK and SPR acknowledge support from EU (contract MEIF-CT-2006-025047) and from the German Academic Exchange Service (DAAD, grant D/06/41156), respectively. This work is supported by Région Île de France (IFRAF), CNRS, the French Ministry of Research, ANR (Project GASCOR, NT05-2-42103) and the EU project SCALA. Laboratoire Kastler Brossel is a research unit of École Normale Supérieure, Université Pierre and Marie Curie and CNRS.

Appendix. The time-of-flight in the 2D MF approximation

We have emphasized in this paper that the measured density profiles differ from those calculated for an ideal gas or within the 2D MF theory. The profiles calculated in steady-state in the trap are found to be much 'peakier' than the experimental ones. As the experimental profiles were actually measured after a time-of-flight of $t = 22\,\mathrm{ms}$ ($\omega_x t = 1.3$), it is important to check that this mismatch between predicted and observed profiles remain valid when the ballistic expansion of the atoms is taken into account. Also the atom distributions were measured using an absorption imaging technique, with an imaging beam propagating along the y-axis. Therefore the measurement gave access to the column density $n_{\mathrm{col}}(x, t)$, obtained by integrating the total density along y. In this appendix, we take into account the time-of-flight and the integration along the y-direction, both for an ideal and for an interacting gas within the 2D MF approximation.

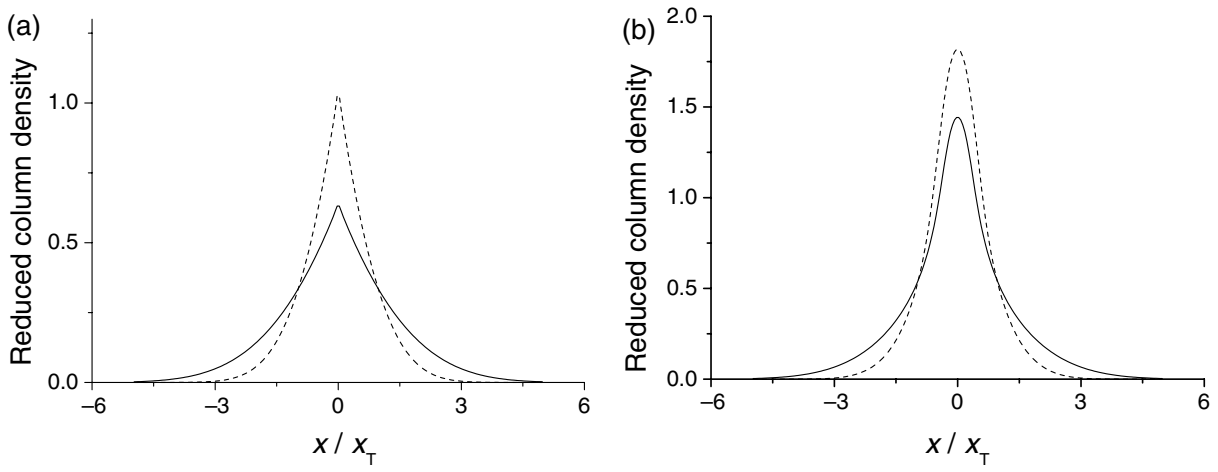

Figure A1. Reduced column density F in the trap (dashed line) and after a time-of-flight t such that $\omega_x t = 1.3$ (continuous line). (a) Ideal gas case, for an atom number equal to the critical value (3). (b) MF result for $\tilde{g} = 0.13$. The fugacity is chosen such that the threshold for superfluidity (11) is met at the center of the trap.

The spatial distribution $n(\mathbf{r}, t)$ at time t can be calculated from the phase space distribution $\rho(\mathbf{r}, \mathbf{p})$ at initial time using

$$n(\mathbf{r}, t) = \int \rho(\mathbf{r} - \mathbf{p}t/m, \mathbf{p}) \mathrm{d}^2 p. \tag{A.1}$$

In the semi-classical approximation the in-trap phase space density is given by

$$\rho(\mathbf{r}, \mathbf{p}) = \frac{1}{h^2} \left\{ \exp\left[\left(p^2/(2m) + V_{\mathrm{eff}}(\mathbf{r}) - \mu \right) / k_{\mathrm{B}} T \right] - 1 \right\}^{-1} \tag{A.2}$$

where $V_{\mathrm{eff}} = V(\mathbf{r}) + 2gn(\mathbf{r})$ and $n(\mathbf{r})$ is obtained by solving (13). The result for the column density can be written as

$$n_{\mathrm{col}}(x, t) = \frac{1}{x_T} \left(\frac{k_{\mathrm{B}} T}{\hbar \omega} \right)^2 F(X, Z, \tilde{g}, \tau), \quad X = \frac{x}{x_T}, \quad \tau = \omega_x t. \tag{A.3}$$

The results for F are shown in figure A1(a) for an ideal gas, and in figure A1(b) for an interacting gas in the MF approximation. In the ideal gas case, the initial column density can be calculated analytically:

$$F(X, Z, 0, 0) = \frac{1}{\sqrt{2\pi}} g_{3/2}\left(Z \mathrm{e}^{-X^2/2} \right) \tag{A.4}$$

and the column density after time-of-flight is deduced from the initial value by a simple dilatation

$$F(X, Z, 0, \tau) = \frac{1}{\sqrt{1+\tau^2}} F\left(\frac{X}{\sqrt{1+\tau^2}}, Z, 0, 0 \right). \tag{A.5}$$

In figure A1(a), the fugacity is such that the atom number equals the critical number (3). In the interacting case of figure A1(b), the number of atoms is such that the criterion for superfluidity is met at the center of the trap. In all cases, it is clear that the observed profiles are very different from a Gaussian, in clear disagreement with the experimental observation.

References

[1] Peierls R E 1935 Quelques propriétés typiques des corps solides *Ann. Inst. H Poincaré* **5** 177
[2] Penrose O and Onsager L 1956 Bose–Einstein condensation and liquid helium *Phys. Rev.* **104** 576
[3] Hohenberg P C 1967 Existence of long-range order in one and two dimensions *Phys. Rev.* **158** 383
[4] Mermin N D and Wagner H 1966 Absence of ferromagnetism or antiferromagnetism in one- or two-dimensional isotropic Heisenberg models *Phys. Rev. Lett.* **17** 1307
[5] Berezinskii V L 1971 Destruction of long-range order in one-dimensional and two-dimensional system possessing a continous symmetry group - ii. Quantum systems *Sov. Phys.—JETP* **34** 610
[6] Kosterlitz J M and Thouless D J 1973 Ordering, metastability and phase transitions in two dimensional systems *J. Phys. C: Solid State Phys.* **6** 1181
[7] Bishop D J and Reppy J D 1978 Study of the superfluid transition in two-dimensional ^{4}He films *Phys. Rev. Lett.* **40** 1727–30
[8] Görlitz A *et al* 2001 Realization of Bose–Einstein condensates in lower dimensions *Phys. Rev. Lett.* **87** 130402
[9] Rychtarik D, Engeser B, Nägerl H-C and Grimm R 2004 Two-dimensional Bose–Einstein condensate in an optical surface trap *Phys. Rev. Lett.* **92** 173003
[10] Smith N L, Heathcote W H, Hechenblaikner G, Nugent E and Foot C J 2005 Quasi-2D confinement of a BEC in a combined optical and magnetic potential *J. Phys. B: At. Mol. Opt. Phys.* **38** 223
[11] Colombe Y, Knyazchyan E, Morizot O, Mercier B, Lorent V and Perrin H 2004 Ultracold atoms confined in rf-induced two-dimensional trapping potentials *Europhys. Lett.* **67** 593
[12] Burger S, Cataliotti F S, Fort C, Maddaloni P, Minardi F and Inguscio M 2002 Quasi-2D Bose–Einstein condensation in an optical lattice *Europhys. Lett.* **57** 1
[13] Köhl M, Moritz H, Stöferle T, Schori C and Esslinger T 2005 Superfluid to Mott insulator transition in one, two, and three dimensions *J. Low Temp. Phys.* **138** 635
[14] Orzel C, Tuchmann A K, Fenselau K, Yasuda M and Kasevich M A 2001 Squeezed states in a Bose–Einstein condensate *Science* **291** 2386
[15] Spielman I B, Phillips W D and Porto J V 2007 The Mott insulator transition in two dimensions *Phys. Rev. Lett.* **98** 080404
[16] Hadzibabic Z, Stock S, Battelier B, Bretin V and Dalibard J 2004 Interference of an array of independent Bose–Einstein condensates *Phys. Rev. Lett.* **93** 180403
[17] Hadzibabic Z, Krüger P, Cheneau M, Battelier B and Dalibard J 2006 Berezinskii–Kosterlitz–Thouless crossover in a trapped atomic gas *Nature* **441** 1118–21
[18] Krüger P, Hadzibabic Z and Dalibard J 2007 Critical point of an interacting two-dimensional atomic Bose gas *Phys. Rev. Lett.* **99** 040402
[19] Posazhennikova A 2006 Weakly interacting, dilute Bose gases in 2D *Rev. Mod. Phys.* **78** 1111
[20] Bloch I, Dalibard J and Zwerger W 2007 Many-body physics with ultracold gases *Preprint* 0704.3011
[21] Schweikhard V, Tung S and Cornell E A 2007 Vortex proliferation in the Berezinskii–Kosterlitz–Thouless regime on a two-dimensional lattice of Bose–Einstein condensates *Phys. Rev. Lett.* **99** 030401
[22] Bagnato V S and Kleppner D 1991 Bose–Einstein condensation in low-dimensional traps *Phys. Rev.* A **44** 7439–41
[23] Prokof'ev N V, Ruebenacker O and Svistunov B V 2001 Critical point of a weakly interacting two-dimensional Bose gas *Phys. Rev. Lett.* **87** 270402
[24] Holzmann M and Krauth W 2007 Kosterlitz–Thouless transition of the quasi two-dimensional trapped Bose gas *Preprint* 0710.5060
[25] Petrov D S, Holzmann M and Shlyapnikov G V 2000 Bose–Einstein condensation in quasi-2D trapped gases *Phys. Rev. Lett.* **84** 2551
[26] Petrov D S and Shlyapnikov G V 2001 Interatomic collisions in a tightly confined Bose gas *Phys. Rev.* A **64** 012706

[27] Dalfovo F S, Pitaevkii L P, Stringari S and Giorgini S 1999 Theory of Bose–Einstein condensation in trapped gases *Rev. Mod. Phys.* **71** 463
[28] Bhaduri R K, Reimann S M, Viefers S, Ghose Choudhury A and Srivastava M K 2000 The effect of interactions on Bose–Einstein condensation in a quasi two-dimensional harmonic trap *J. Phys. B: At. Mol. Opt. Phys.* **33** 3895
[29] Fernández J P and Mullin W J 2002 The two-dimensional Bose–Einstein condensate *J. Low Temp. Phys.* **128** 233
[30] Gies C and Hutchinson D A W 2004 Coherence properties of the two-dimensional Bose–Einstein condensate *Phys. Rev.* A **70** 043606
[31] Petrov D S, Gangardt D M and Shlyapnikov G V 2004 Low-dimensional trapped gases *J. Physique* IV **116** 5–44
[32] Simula T P and Blakie P B 2006 Thermal activation of vortex–antivortex pairs in quasi-two-dimensional Bose–Einstein condensates *Phys. Rev. Lett.* **96** 020404
[33] Nelson D R and Kosterlitz J M 1977 Universal jump in the superfluid density of two-dimensional superfluids *Phys. Rev. Lett.* **39** 1201
[34] Popov V N 1983 *Functional Integrals in Quantum Field Theory and Statistical Physics* (Dordrecht: Reidel)
[35] Kagan Y, Svistunov B V and Shlyapnikov G V 1987 Influence on inelastic processes of the phase transition in a weakly collisional two-dimensional Bose gas *Sov. Phys.—JETP* **66** 314
[36] Fisher D S and Hohenberg P C 1988 Dilute Bose gas in two dimensions *Phys. Rev.* B **37** 4936
[37] Al Khawaja U, Andersen J O, Proukakis N P and Stoof H T C 2002 Low dimensional Bose gases *Phys. Rev.* A **66** 013615
[38] Holzmann M, Baym G, Blaizot J P and Laloë F 2007 Superfluid transition of homogeneous and trapped two-dimensional Bose gases *Proc. Natl Acad. Sci. USA* **104** 1476
[39] Prokof'ev N V and Svistunov B V 2002 Two-dimensional weakly interacting Bose gas in the fluctuation region *Phys. Rev.* A **66** 043608
[40] Holzmann M 2007 private communication
[41] Kadanoff L P and Baym G 1963 *Quantum Statistical Mechanics* (New York: Benjamin-Cummings)
[42] Holzmann M, Chevalier M and Krauth W 2008 Semiclassical theory of the quasi two-dimensional trapped gas *Preprint* 0801.2758
[43] Bramwell S T and Holdsworth P C W 1994 Magnetization: a characteristic of the Kosterlitz–Thouless–Berezinskii transition *Phys. Rev.* B **49** 8811–4